Desalination and Water Treatment
www.deswater.com

doi: 10.5004/dwt.2022.28398

257 (2022) 76–90
May

Modeling of fluoride removal by nanofiltration: coupled film theory model with Nernst–Planck equation and artificial neural network

F.Z. Addar[a], B. Fahid[b], M. Belfaquir[a], M. Tahaikt[a], A. Elmidaoui[a], M. Taky[a,c,*]

[a]*Laboratory of Advanced Materials and Process Engineering, Faculty of Sciences, Ibn Tofail University, P.O. Box 1246, Kenitra – Morocco, emails: elmidaoui@uit.ac.ma (A. Elmidaoui), mohamed.taky@uit.ac.ma/takymogamed@gmail.com (M. Taky), Fatima.zahra@uit.ac.ma (F.Z. Addar), Mustapha.belfaquir@uit.ac.ma (M. Belfaquir), mustapha.tahaikt@uit.ac.ma (M. Tahaikt)*
[b]*Laboratory of Analysis, Geometry and Applications, Superior School of Technology, Ibn Tofail University, P.O. Box 1246, Kenitra – Morocco, email: brahim.fahid@uit.ac.ma (B. Fahid)*
[c]*International Water Research Institute, Mohammed VI Polytechnic University, Lot 660, Hay Moulay Rachid, Ben Guerir, 43150 – Morocco*

Received 6 January 2022; Accepted 14 March 2022

ABSTRACT

Fluoride ions are necessary and beneficial for human beings, however high levels of fluoride in groundwater can be toxic and harmful to human health and water resources, causing serious problems on teeth and bones. This situation is widespread in many parts of the world, including Morocco. According to World Health Organization (WHO), the maximum allowable concentration of fluoride in drinking water is 1.5 mg/L. The objective of this work is to understand the mechanism of transfer of fluoride ions in nanofiltration (NF) membranes. Two methodologies have been used, one mathematical, Nernst–Planck equation combined with film theory (NP-FT), and the other statistical artificial neural network (ANN). This study has been realized with experimental data obtained from three NF membranes (TR60, NF270 and NF90) that have been used for the removal of fluoride from NaF-doped groundwater with different initial concentrations of 5, 10, 15 and 20 mg/L. In a first part, the NP-FT model that is proposed as a contribution to the modeling of the concentration polarization phenomenon and to study the influence of the initial concentration (C_i) of fluoride on the reflection coefficient (σ), the permeability of the solute (P_s) and the thickness of the boundary layer (δ) has been made. In a second part, the two models ANN and NP-FT are used to predict the fluoride rejection as a function of the permeate flux. In addition, a comparison is made in terms of coefficient of determination R^2 between the two models. The results obtained showed that the influence of concentration bias is more important for NF270 than for TR60 and NF90, and high reflection coefficients, almost equal to unity, were obtained for NF90, indicating that convective transport is almost completely hindered. Similarly, reflection coefficients of about 0.97 and 0.89 were found for TR60 and NF270, respectively, suggesting that both mechanisms are present, but that diffusion is more pronounced for NF270 than for TR60. Thus, the thickness of the boundary layer and permeability change inversely to one another. It is about 10^{-5} m for NF270 and 10^{-6} m for TR60. On the other hand, the value obtained for the NF90 membrane is 10^{-14} m which is very low. The obtained solute permeability follows the order: R60 > NF270 > NF90. Although the experimental data agree well with the data predicted by ANN and NP-FT, which indicates that both models are appropriate for the prediction and satisfactory R^2. However, the ANN model reveals a slight superiority over the NP-FT model.

Keywords: Fluoride removal; Nanofiltration; Artificial neural networks; Modelling; Concentration polarization; Nernst–Planck equation; Film theory

* Corresponding author.

Presented at the Second International Symposium on Nanomaterials and Membrane Science for Water, Energy and Environment (SNMS-2021), June 1–2, 2022, Tangier, Morocco

1. Introduction

Population growth and water scarcity put pressure on available natural water resources. This has been confirmed by (WHO) and United Nations International Children's Emergency Fund (UNICEF) report that millions of people do not have a safe and enough supply of water for drinking and other everyday tasks [1,2]. Groundwater represents only 0.6% of total water ressources and surface water are threatened by pollution from intense industrialization and urbanization activities [3].

The physical presence of many elements and compounds, both natural and anthropogenic, due to the interaction between soil and water, soil–gas interaction, contact of rocks with groundwater and time of residence in aquifers [4], especially fluorides, arsenic, nitrates, sulphates, iron, manganese, chloride, selenium, etc., can significantly affect the quality of water and cause adverse effects on health [5,6].

The issue of high fluoride concentration in groundwater resources has become one of the most serious toxicological and geo-environmental problems in several countries, India is the country most concerned by this problem of fluorides. During the last three decades, higher concentration of fluoride in drinking water and the resulting disease "fluorosis" have been significantly highlighted worldwide. The effect of fluoride in drinking water can be beneficial or deleterious to mankind. The determining parameters are the concentration and the duration of absorption. Thus, when it is present in a narrow concentration range, it plays an imperative role in bone mineralization and also acts as an antibacterial agent in the mouth. On the contrary, an excessive concentration (3–6 mg/L) of fluoride can have a negative effect on bones and teeth (dental and skeletal fluorosis) [7]. Absorption of excess fluoride (>10 mg/L) in the human body can cause dental, skeletal and non-skeletal "fluorosis". Similarly, lack of fluoride in groundwater (less than 0.5 mg/L) can cause dental caries which is why the WHO has fixed a maximum concentration of fluoride in drinking water of 1.5 mg/L [8].

In Morocco, fluoride levels exceed acceptable standards in several regions, for instance, the Ben Guerir Plateau (Central Morocco). The water in this region generally exceeds the fluoride standards of 2 to 3 mg/L. This contamination is due to the deposition of phosphate [9,10].

A multitude of conventional and non-conventional methods have been implemented for water defluoridation, namely adsorption [11,12], ion-exchange [13], electrodialysis (ED) [11], precipitation/coagulation [14], electroagulation [15,16], and pressure-driven membrane-based technologies as nanofiltration (NF) and reverse osmosis (RO) [17–19].

Many studies have shown that NF in groundwater defluoridation is cost-effective makes it economically and operationally attractive [20,21]. Pontié et al. [22] employed a polyamide NF45 membrane (FilmTec), they obtained a fluoride rejection of 91% at 0.02 mol/L of NaF in the feed. Nasr et al. [23] examined the commercial NF5 and NF9 membranes (Manufactured by Applied Membranes Inc, USA) to remove fluoride ions from Tunisian groundwater with fluoride concentration around 3 mg/L. NF9 exhibited a better rejection of (88%) than NF5 (57%) with fluoride concentrations in the permeate of 0.38 and 1.45 mg/L respectively. Mnif et al. [24] studied the defluoridation of aqueous solutions exceeding 1.5 mg/L using a thin film polyamide NF composite membrane called HL 2514 T, manufactured by GE-Osmonics (USA). The results showed that the fluoride rejection by the HL membrane was over 80% at a permeate fluoride concentration of 2×10^{-2} mol/L.

Since the separation mechanism of NF membranes is very complex, several models have been established to illustrate and predict the flux and retention of a variety of species under different operating conditions [25]. The most applied models are Kedem–Katchalsky [26,27], Spiegler–Kedem [26–28] and models based on the Nernst–Planck equation [29].

In a previous study, Addar et al. [9], used statistical model to optimize the fluoride removal process by three NF membranes and applied surface response methodology (RSM) based on a central composite design (CCD), minimizing the permeate concentration and maximizing the fluoride rejection and permeate flux. Optimal conditions to obtain water that meets the standards set by WHO of the two membranes TR60, NF270 were determined: fluoride concentration in the feed lower than 7 and 5.5 mg/L and operating transmembrane pressure (TMP) of 10 and 13 bars respectively. Whereas, for NF90, the fluoride feed concentration has no influence on the fluoride rejection and the fluoride contents obtained in the permeate were well below the standards. In addition, Tahaikt et al. [18], investigated the influence of initial fluoride concentration on the transfer of fluoride by applying the Spiegler–Kedem and Kedem–Katchalsky models while neglecting electrical interactions and concentration polarization layer. The results showed that NF270 and TR60 involved two different mechanisms: diffusion and convection with the preponderance of diffusion. On the other hand, for NF90, the transfer mechanism is close to that of RO.

Other mathematical models can be used to improve the understanding of the fluoride transfer in NF membranes by taking into account the previously neglected phenomena such as film theory coupled to the Nernst–Planck equation which accounts for concentration polarization layer splicing. Concentration polarization is a reversible phenomenon that takes place when the rejected solutes accumulate on the membrane surface, creating a local concentration, much higher than that of the feed solution and which is very difficult to be experimentally determined. This phenomenon has negative effects on membrane performance, including reduced flux and increased membrane fouling [30]. As a consequence, there is a need to find an alternative way to predict NF process performance by exploiting the available data and extending it to unavailable data. The extended Nernst–Planck model coupled with film theory (NP-FT) and artificial neural networks (ANNs) is capable of modeling highly complex and nonlinear systems for NF membranes [25].

The mathematical model used is a coupled model of Nernst–Planck equation and the film theory proposed by Chaabane et al. [30]. It is a combination of the model based on the extended Nernst–Planck equation which is widely used in the literature to describe the transport of ionic species in membrane separation systems and the

film theory equation to describe the mechanism of solute transfer in the concentration polarization layer [30,31]. This model is characterized by three parameters: reflection coefficient σ, solute permeability P_s and boundary layer thickness δ [32].

ANNs have received a lot of attention, largely due to their wide range of applications and the ease with which they handle large numbers of applications and complex and highly nonlinear data. Once the ANN is trained with experimental data, it can be used in a purely predictive mode to calculate the dependent variable(s) for any value of the input variables. Process modeling is an area in which ANNs of various configurations and structures have been considered as effective tools [33–35]. On the other hand, ANNs provide a more attractive alternative to the classic "black box" models for dealing with complex phenomena. ANNs successfully apply to different types of membranes: microfiltration (MF), ultrafiltration (UF) and NF [25,35–39]. For instance, Bowen et al. [39] applied ANN to provide a means of modeling the performance of the NF process, thus used ANN to predict the rejection of single salts (NaCl, Na_2SO_4, $MgCl_2$ and $MgSO_4$) and mixtures of these salts at a spiral rolled NF membrane. They found good agreement between ANNs predictions and experimental data single salts and mixtures.

In this study, two methodologies, one statistical (ANN) and the other mathematical, extended NP-FT are used to predict and explain the variation of fluoride rejection as a function of permeate flux for three NF membranes (NF90, NF270 and TR60) considering four initial concentrations. The NP-FT model is used to determine the reflection coefficient σ, the solute permeability P_s, and the boundary layer thickness δ, including the concentration polarization phenomenon. While the ANN model is applied to provide a means of modeling the performance of the studied membranes. To compare the predictive power of the two models, the values of the determination coefficient R^2 are calculated for the validity. Finally, a comparison between the two models in the fitting of fluoride rejection data with the permeate flux is performed.

2. Experimental

2.1. Characteristics of the feed water

The experiments are conducted on groundwater doped by NaF at different concentrations. A very slight variation of pH and conductivity was observed. The analytical results of the feed water are presented in Table 1.

2.2. Unit pilot testing

The experiments are performed on an NF/RO pilot plant (E 3039) supplied by TIA Company (Technologies Industrielles Appliquées, France) shown in Fig. 1. The applied TMP can vary in the range of 5–70 bar using manual valves.

The pilot plant is equipped with two identical pressure vessel operating in series. Each pressure vessel contains one element. The pressure loss is about 2 bar corresponding to 1 bar of each pressure vessel. The two spiral wound modules are equipped with two identical commercial membranes. The water to be treated is taken from the tank by a pump and introduced into the first fissel, the retentate is admitted into the second fissel and the two permeates are recovered and mixed.

The washing is carried out by a basic solution of sodium hydroxide NaOH at pH between 9 and 10 for 10 min, followed by a rinse with water, then a washing with a solution of sulfuric acid $H_2SO_4^{2-}$ at pH between 3 and 4 for 15 min.

The temperature is kept at 29°C using the heat exchanger. Samples of permeate are collected and water parameters are determined analytically following standard methods previously described [19,42]. The other parameters followed are:

The permeate flux is given by the equation [43,44]:

$$J_v = \frac{Q_p}{S}\left(\frac{\mathrm{L}}{\mathrm{m}^2\cdot\mathrm{s}} \text{ or } \frac{\mathrm{m}^3}{\mathrm{m}^2\cdot\mathrm{s}}\right) \quad (1)$$

where S is the membrane surface area (m^2) and Q_p the flow rate of the permeate (L/h or m^3/s).

Table 1
Characteristics of the feed water

Parameters	Feed water	Moroccan guidelines [40]	WHO standards [41]
Temperature (°C)	29	–	–
Turbidity, NTU	<2	–	–
pH	7.41 ± 0.03	6–9.2	6.5–8.5
pHs	7.80 ± 0.05	–	–
Electric conductivity, μS/cm	1,492 ± 26	2700	–
Hardness, mg/L $CaCO_3$	440 ± 8	500	500
Alkalinity, mg/L $CaCO_3$	320 ± 10	200	–
Fluoride, mg/L	5–10–15–20 ± 0.6	1.5	1.5
Sulphate, mg/L	116 ± 4	200	200
Nitrate, mg/L	20 ± 0.5	50	50
Chloride, mg/L	560 ± 10	750	250
Sodium, mg/L	246 ± 15	–	–

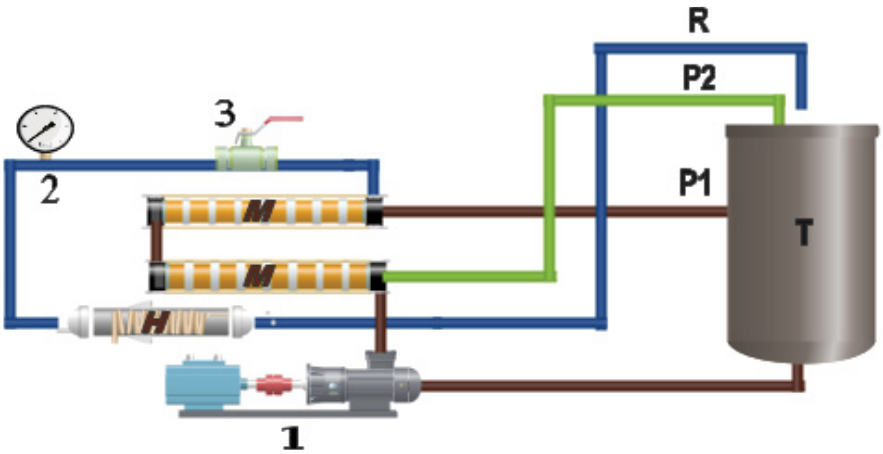

Fig. 1. Schematic diagram of the NF/RO pilot plant [9]. T: Tank; M: NF module; P: Permeate recirculation; R: Retentate recirculation; H: Heat exchanger; 1: High pressure pump; 2: Pressure sensor. 3: Pressure regulation valves.

The recovery rate (Y) is defined as:

$$Y(\%) = \frac{Q_p}{Q_0} \times 100 \quad (2)$$

where Q_p is the permeate flow (L/h) and Q_0 the feed flow (L/h).

Salt rejection (R) is defined as:

$$R = \left(1 - \frac{C_p}{C_0}\right) \times 100 \quad (3)$$

where C_p is the solute concentration in permeate (g/L) and C_0 the solute concentration in the feed water (g/L).

2.3. Characteristics of the membranes

The two spiral wound modules are equipped with two identical commercial NF membranes. Table 2 gives the characteristics of the membranes used. After the run, the membranes are cleaned with alkaline and acidic cleaning solutions according to the manufacturer recommendations.

2.4. Application of ANN

The feed-forward, back propagation network (FFBPN) model is constructed in this study. In the initial phase, the model is trained using the available historical data. If the model does not meet expectations, it is then used to propagate the process until it reaches the best requirement using the Levenberg–Marquardt (LM) backpropagation algorithm [46]. The network is composed of three layers, namely the input, hidden and output layers. The proposed network has been used by the sigmoid function (logsig + tansig) in the hidden layer and the linear function (Purelin) in the output layer. The input layer receives the input signals from the other source [47]. On the other hand, ANN algorithms, programmed in the Matlab toolbox for neural networks, are used to predict variation of the fluoride rejection as a function of permeate flux for the three different NF membranes used in this work. The input data of the ANN network are the permeate flux while the output

Table 2
Characteristics of the membranes used

	NF270**4040	NF90*4040	TR60*4040
Area (m^2)	7.6	7.6	6.8
Salt rejection (%)	>97.0%	97%	–
P_{max} (bar)	41	41	10
Material	Polyamide	Polyamide	Polyamide
Contact angle (°) [45]	27	54	–
Zeta potential (mV) [45]			
pH = 3	4.9	3.7	–
pH = 12	–25.6	–19.4	–

- Salt rejection based on the following test conditions 2,000 ppm $MgSO_4$, 77°F (25°C), and 15% recovery rate at the pressure 4.8 bar.
- Salt rejection based on the following test conditions 2,000 ppm NaCl, 77°F (25°C), and 15% recovery rate at the pressure 10 bar.
- Salt rejection based on the following test conditions 2,000 ppm NaCl, 77°F (25°C), and 15% recovery rate at the pressure 15.5 bar.

is the fluoride rejection which are available for four concentrations, 5, 10, 15, and 20 mg/L.

3. Theoretical background of modeling methods

3.1. Extended Nernst–Planck equation coupled with film theory

The model used in this article is described by Chaabane et al. [30] and based on the extended Nernst–Planck equation simplified by Dresner [48], which can be written as follows:

$$J_i = -P_i^* \left(\frac{dC_i}{dx} + \frac{FZ_iC_i}{RT}\frac{d\Psi}{dx} \right) + J_iC_i\left(1-\sigma_i\right) \tag{4}$$

Rearrangement of equation with the electroneutrality conditions:

$$\sum_i Z_iC_i = 0$$
$$\sum_i J_iC_i = 0 \tag{5}$$

Z_i is the ion valence. Give the Kedem–Speigler equation:

$$J_i = -P\frac{dC_i}{dx} + J_iC_i\left(1-\sigma_i\right) \tag{6}$$

Eq. (6) is integrated over the membrane thickness ($0 < x < \Delta x$) using the following boundary conditions:

For $x = 0$, $C_m = C_f$ and for $x = \Delta x$, $C_m = C_p$.

$$C_f = \left\{ 1 - \frac{\sigma}{\exp\left[\frac{J_v(1-\sigma)}{p_s}\right]} \right\} \frac{C_p}{1-\sigma} \tag{7}$$

Taking into account concentration polarization phenomena which occurs in a boundary layer adjacent to the membrane/feed solution interface where the cross-flow velocity is essentially laminar and the backward transport of the retained solute is by diffusion. The thickness of the polarization layer δ can vary from a few microns to hundreds of microns, depending on factors such as the nature of the feed solution, module design, cross-flow rate and TMP [49,50].

In the steady state, and according to the film theory [51–53], the convective transport of solute across the membrane is therefore equivalent to the diffusive back-transport of the solute plus that passing with the permeate Jc_p the following mass balance can be constructed:

$$J_vC_p = J_vC_f - D_s\frac{dc}{dx} \tag{8}$$

Integration of Eq. (8) over the thickness of the boundary layer results in:

$$\frac{C_f - C_p}{C_0 - C_p} = \exp\left(\frac{J_v}{Q}\right) \quad \text{with} \quad Q = \frac{D_S}{\delta} \tag{9}$$

where Q is the mass transfer coefficient.

The observed retention (R_{obs}) of fluoride can be written as follows:

$$R_{obs} = 1 - \frac{C_p}{C_0} \tag{10}$$

With Eqs. (7) and (9), R_{obs} can be given by:

$$R_{real} = 1 - \frac{1}{1 + \frac{\sigma}{1-\sigma}\left\{ \exp\left(\frac{-J_v\delta}{D_S}\right) - \exp\left(\frac{-J_v(1-\sigma)}{p_s} - \frac{J_v\delta}{D_S}\right)\right\}} \tag{11}$$

Fig. 2 shows this case, assuming no fouling layer is present on the membrane/supply interface [54].

3.2. ANN approach

ANNs provide a rich framework for modeling nonlinear phenomena and for solving multivariate regression problems [25]. The ANN is a processing system composed of neurons (nodes) and connections between them that can be used to map input and output data, where the factors are called inputs and the response is called target (experimental response) or output (predicted response) [55]. According to the theory of universal approximation, a functional relationship between an arbitrary number of input variables and an arbitrary number of output variables can be constructed by an ANN with only two layers (an input layer, a hidden layer and an output layer), whose transfer function of the hidden layer is nonlinear and whose transfer function of the output layer is purely linear. The transfer functions compute the output of a layer from its net input and contain log-sigmoid (logsig), tan-sigmoid (tansig) and pure linear (purlin) functions [56,57]. There are several ANN models such as the feed-forward model, the multilayer perceptron (MLP) and the radial basis function (RBF) [25].

Our study includes the use of FFBPN network due to the ability of this method to modeling any function. Fig. 3 shows the general structure of the FFBPN model. Moreover, learning rule FFBPN is used to adjust the weight values and threshold values of a system to obtain the minimum error [58]. In addition, the input neurons received the experimental data and the network provided its outputs (ANN simulation data). If the output of the ANN network is not equal to the experimentally measured outputs, our procedure calculates the mean square error between the two values and modified the ANN network weights to minimize it. The training data are normalized to the interval [0–1]. Sixty percent of the collected data are used for model training, while 30% of the data is equally divided for testing and validation, respectively. The model is then trained based on Eq. (11) until the total mean square error is (or becomes) minimal [58].

$$x_J = \sum_i^n W_{ji}x_i \tag{12}$$

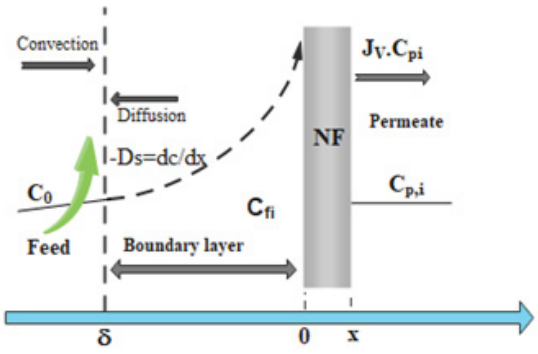

Fig. 2. Conditions of the boundary layer at the membrane/supply interface.

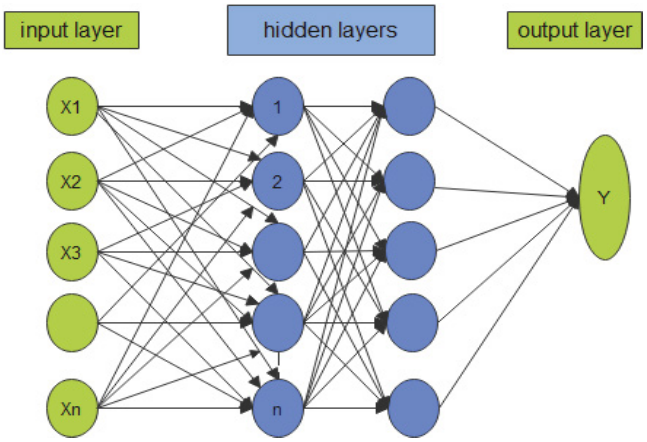

Fig. 3. Proposed neural network architecture.

where x_j is the variable's new value, x_i is the variable's initial value and W_{ji} is the neuron/variable's weight link value. The activation function between the input and the hidden layer is (tansig) and log-sigmoid (logsig), as indicated by Eq. (12).

$$f(x)=\frac{e^{x}-e^{-x}}{e^{x}+e^{-x}} \quad \text{and} \quad f(x)=\frac{1}{1+e^{-x}} \tag{13}$$

The purelin function is used as Eq. (13) between the hidden layer and the output layer:

$$f(x)=x \tag{14}$$

Finally, the reliability of the model is validated with a new (unknown) data set and the results are found to be satisfactory. The rationale for these steps is discussed in the results section.

4. Results and discussion

In previous study [9], RSM statistical method was used for optimizing the defluorination operation using three membranes (TR60, NF270 and NF90). Furthermore, two theoretical models Spiegler–Kedem and Spiegler–Katchalsky were used to explain the ion transfer across these membranes [18]. The objective of this work is to test the extended Nernst–Planck model coupled with film theory (NP-FT) that accounts for the polarization layer is used to determine the phenomenological parameters of the models, namely the reflection coefficient σ, the solute permeability P_s and δ, the thickness of the boundary layer. In addition, the ANN model is also used to predict the fluoride rejection as a function of permeate flux. Finally, a comparison between the two models will be highlighted.

4.1. Nernst–Planck modeling coupled with film theory

4.1.1. Effect of transmembrane pressure

The variation of the permeate fluoride content and the permeate flux (Fig. 4) as a function of TMP is studied in batch mode and for a groundwater from the Ben Guerir region doped with different fluoride concentrations, already published in our previous paper [9,18].

As shown in Fig. 4, the permeate flux increases almost linearly with TMP according to Darcy's law [59]. This flow behavior is well established in the literature [9,10,18]. In this illustration, the permeate flux follows the following order: NF270 > TR60 > NF90. Namely that the permeability of solvent water found 5.58×10^{-6}; 1.15×10^{-6}; 2.49×10^{-6} m^3/m^2 s bar for NF270, NF90, TR60 respectively. For all three membranes studied, fluoride passage into the permeate increases with increasing initial feed fluoride content and decreases with increasing TMP, except for NF270, a slight increase is observed for TMP above 10 bar.

4.1.2. Parameters of the model

The applied model, NP-FT has been used to study the influence of the initial fluoride concentration of the feed on the reflection coefficient (σ), the solute permeability (P_s) and the boundary layer thickness (δ) taking into account the concentration polarization phenomenon. For this aim, a program in Python language has been developed on the basis of the flowchart (Fig. 5) proposed by Chaabane et al. [30]. The results obtained from the model simulation are used to plot the curves in the Origin software depicted in Fig. 6. The experimental data obtained experimentally are indicated by solid symbols, while the solid lines represent the function of the model with the parameters found by the program. A summary of the calculated model parameters are collected in Table 3.

Fig. 6 shows, for the studied membranes, and for the range of initial fluoride concentrations, a good fit of fluoride rejection obtained experimentally and by the NP-FT model. The obtained *R*-squared values confirm this accordance.

The calculated reflection coefficients are almost equal to unity for NF90. For NF270, the values found exceed 0.97 which are higher than those found in the paper by Tahaikt et al. [18], where the concentration polarization was neglected. For TR60, σ is around 0.89 which is almost the same value obtained previously by Tahaikt et al. [18]. This indicates that the influence of concentration polarization is more important for NF270 than for TR60 and NF90. The high reflection coefficients indicate that convective transport in the NF90 membrane is almost completely hindered. In addition, these results could be explained on the basis of

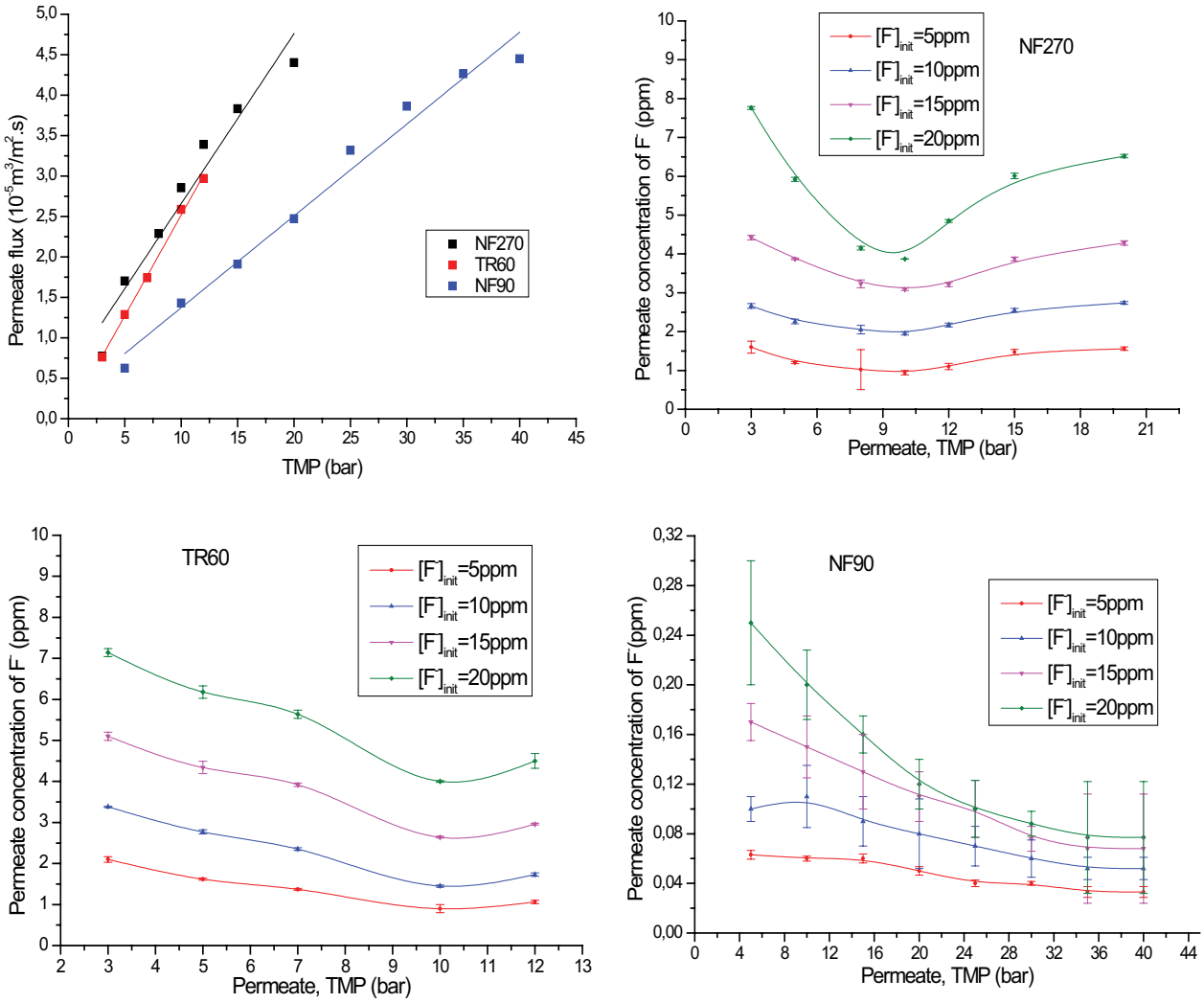

Fig. 4. Effect of TMP on fluoride content and permeate flux for the three membranes [9,18].

the steric hindrance mechanism, since NF90 has relatively small pores, as shown by atomic force microscopy [25]. For TR60 and NF270, both diffusive and convective mechanisms are present, but the predominance of diffusion is more pronounced for NF270 than for TR60. On the other hand the boundary layer thickness for NF270 is 10 times larger than that of TR60 which means that NF270 retains more fluoride.

The results obtained show that the greater the thickness layer, the lower the permeability. δ is about 10^{-5} m for NF270 and 10^{-6} m for TR60. On the other hand, the obtained δ for NF90 is 10^{-14} m which is very low or even non-existent. This explains the order of the solute permeability: TR60 > NF270 > NF90. However, the values obtained for either δ and P_s are very low.

The formation of the boundary layer is generally due to the accumulation of the retained solute on the membrane surface, which is a function of the flow of the permeate. The lower the concentration of fluoride on the surface of the membrane, the lower the thickness of the boundary layer. In reality, during NF, other phenomena are involved in the formation of the boundary layer, such as the dielectric exclusion effect, the electrical interaction between the charged membrane surface and the solvent as well as the screen effect, which occurs when the concentration of different ions increases, the counter ions and other retained co-ions form films (also called "screen") near the surface of the membrane, which are able to reduce or eliminate the solute particles [18,30].

The plot of the evolution of P_s and δ (Fig. 7) as a function of the initial fluoride ion concentration shows how these two parameters are influenced slightly by the initial fluoride content for TR60, NF270 and NF90. As shown in Fig. 7, the behavior of these two parameters is almost linear. The increase of the fluoride content in the raw water causes a slight decrease in P_s for NF270 and TR60. On the other hand, for NF90, P_s values are very low and a very slight occurs with increase of fluoride concentration is observed.

Table 3 gives the estimated parameters of the NP-FT model, namely the reflection coefficient (σ), solute permeability (P_s), and boundary layer thickness (δ) considering the concentration polarization phenomenon.

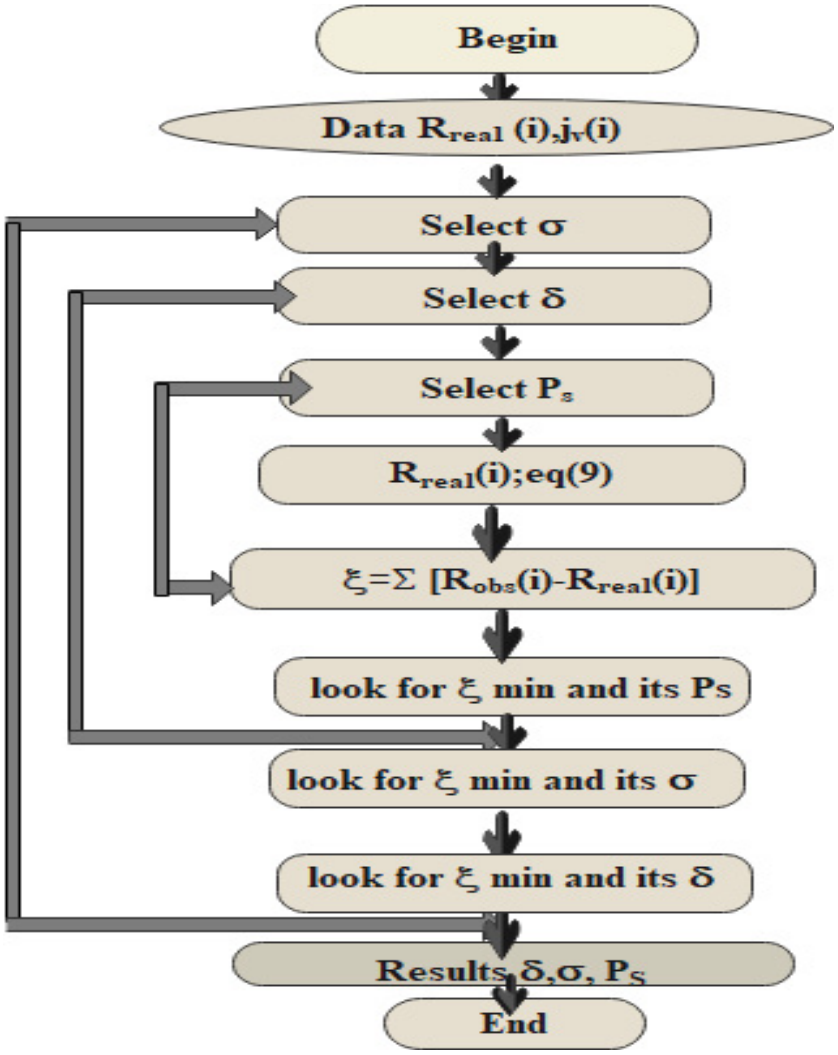

Fig. 5. Program flowchart considering concentration polarization phenomenon.

Table 3
Parameters, σ, P_s and δ obtained by the coupled NP-FT model

Membrane	C_i (ppm)	δ (m)	σ	P_s	R^2
TR60	5	1.6×10^{-6}	0.890	4.90×10^{-6}	0.900
	10	1.6×10^{-6}	0.897	3.28×10^{-6}	0.900
	15	1.4×10^{-6}	0.900	4×10^{-6}	0.800
	20	1.4×10^{-6}	0.800	2.84×10^{-6}	0,880
NF270	5	6.5×10^{-5}	0.980	2.24×10^{-6}	0.700
	10	6.8×10^{-5}	0.970	6.68×10^{-7}	0.760
	15	6.5×10^{-5}	0.970	6.14×10^{-7}	0.750
	20	6×10^{-5}	0.980	4.43×10^{-7}	0.770
NF90	5	3.4×10^{-14}	0.991	5.74×10^{-8}	0.720
	10	3.8×10^{-14}	0.993	4.76×10^{-8}	0.700
	15	1.0×10^{-14}	0.994	6.03×10^{-8}	0.810
	20	4.2×10^{-14}	0.994	6.84×10^{-8}	0.818

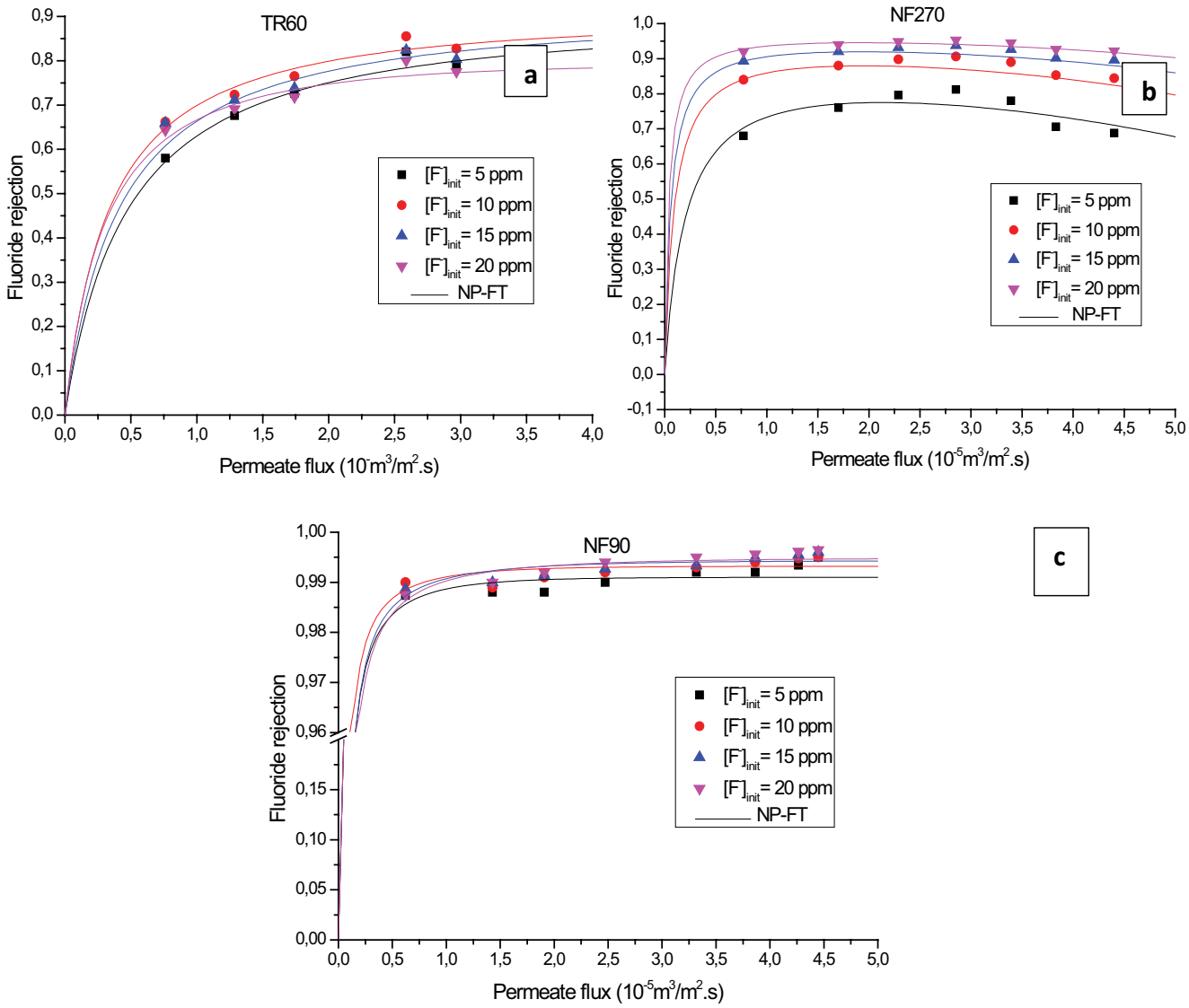

Fig. 6. Experimental and model data of fluoride rejection vs. permeate flux for the three membranes.

4.2. Simulation by ANN

4.2.1. ANN prediction of fluoride rejection as a function of permeate flux

The ANN prediction (Fig. 8) of fluoride rejection as a function of permeate flux for different initial concentrations and for the three NF membranes is performed. The experimental data used in the learning process are indicated by solid symbols, while the solid lines represent the best polynomial fit of the ANN prediction.

Fig. 8 shows the ANN predictions for the fluoride rejection as a function of permeate flux data for the three membranes using different initial fluoride concentrations. It is clear that there is good agreement between the ANN prediction and the experimental data for the three membranes with very little deviation (slight difference). The good prediction by ANN obtained can be explained by the fact that the sweatpants used in the learning phase are relatively few, and the use of other set-points, especially at the level of initial concentration of fluoride intermediate, will certainly improve the interpretive performance of ANN predictions as shown in previous work [25]. The ANN model perfectly describes the fluoride rejection data for TR60, NF270 and NF90 membranes.

4.2.2. Validation of the model ANN

The results obtained for the training, the test, the validation and the global R^2 for the training data set, for the three membranes are depicted in Fig. 9.

The summaries of the R^2 plots during the training, testing, and validation stages during the training process for the three membranes are shown in Fig. 9. In order to evaluate the ANN model, the model is presented with new fluoride rejection values that are not used during training. The fluoride rejection values estimated by the ANN

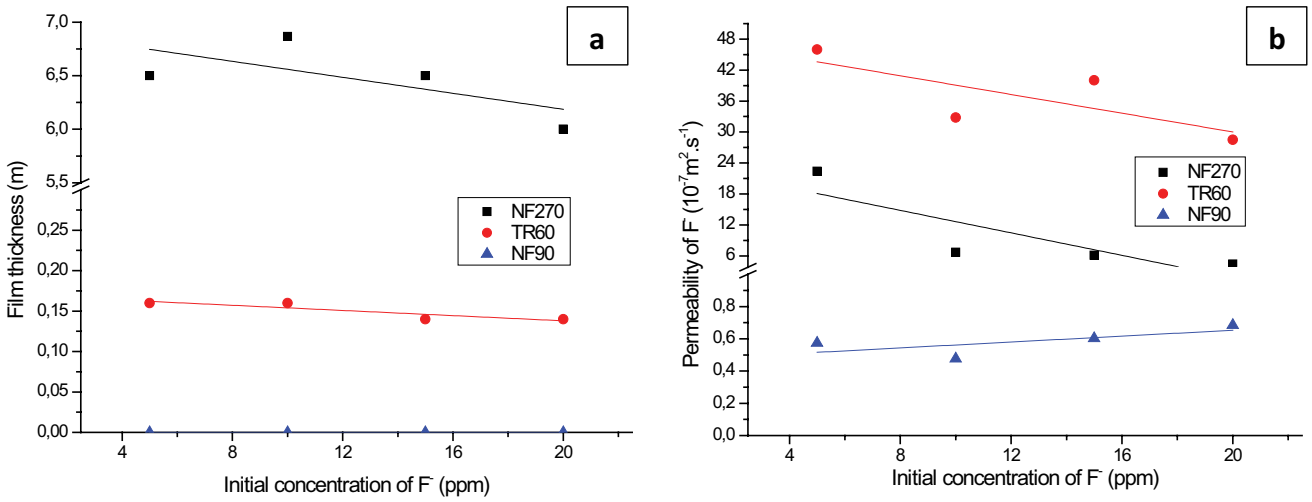

Fig. 7. Variation of permeability (a) and layer thickness (b) as a function of initial fluoride concentration for the three membranes.

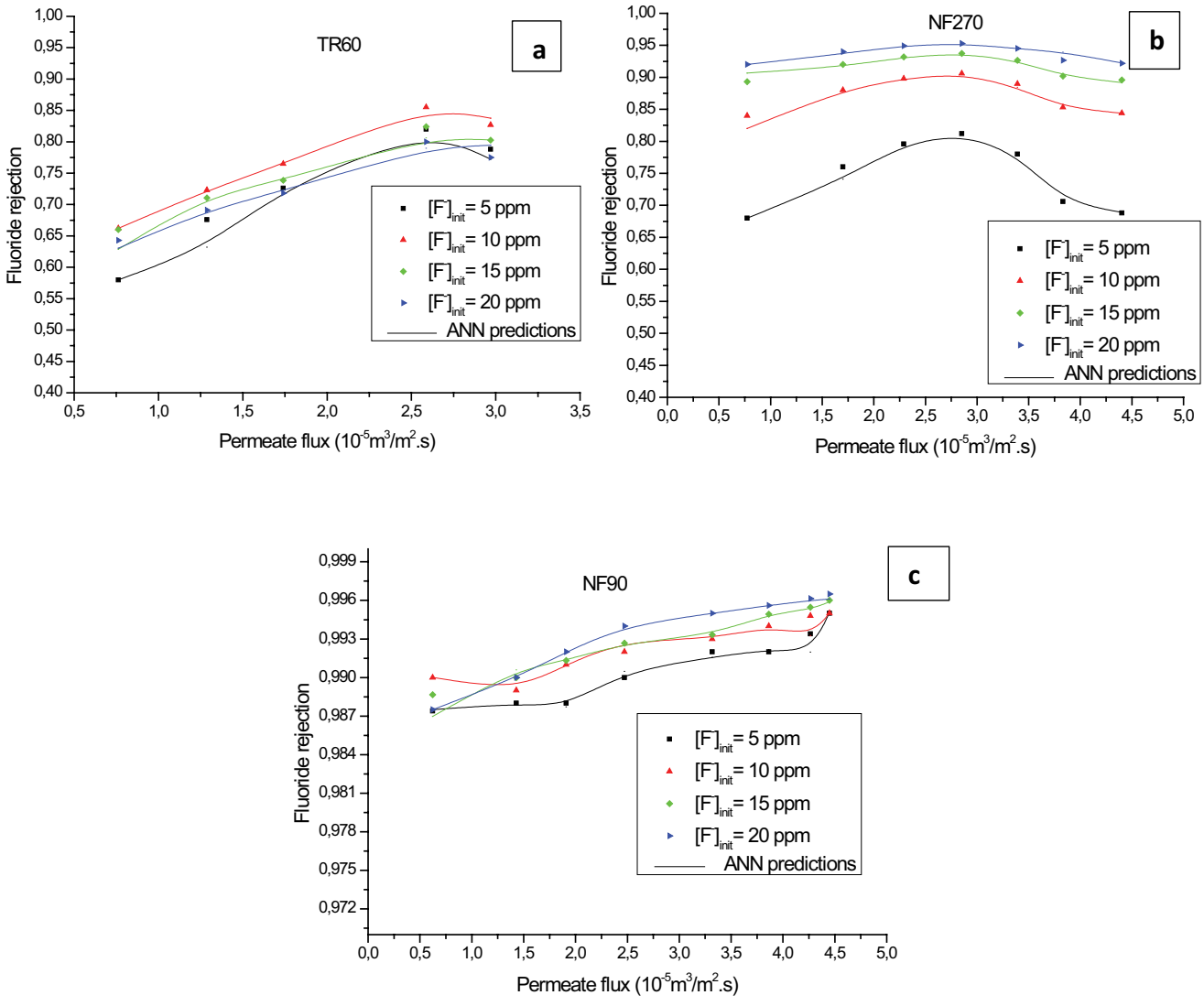

Fig. 8. Experimental and adjustment data by (ANN), fluoride rejection as a function of permeate flux.

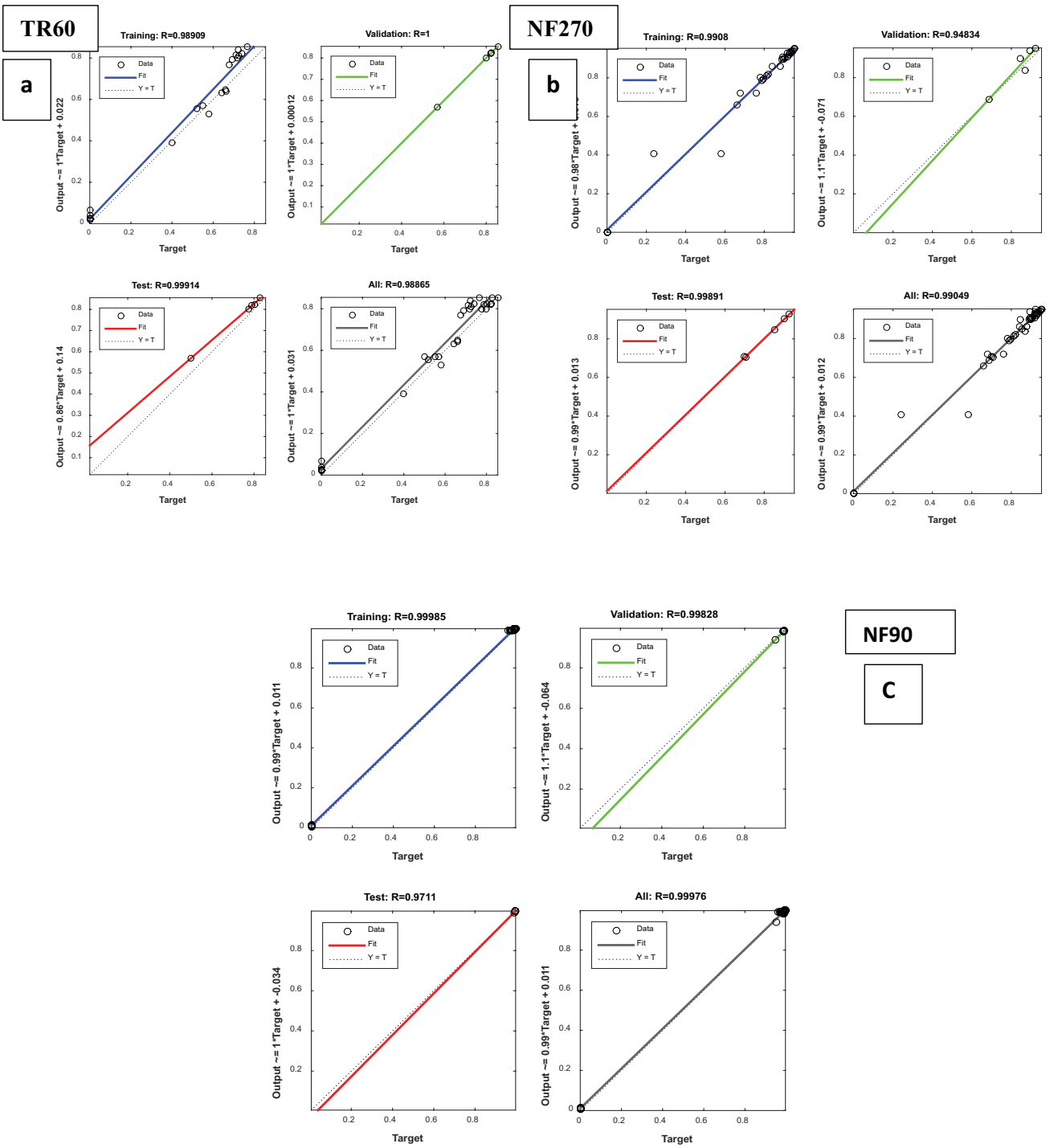

Fig. 9. Network model with training, validation, testing and prediction set for the three TR60, NF270 and NF90 membranes.

model is then compared to their corresponding actual values. An overall R^2 value of 1–0.9483–0.9982 is obtained for TR60, NF270 and NF90, respectively, showing a perfect correlation (output exactly equal to the target). On the other hand, for all curves, the points are located very close to the straight line and the best-fit equations for the training, validation, test, and ensemble subsets have mainly a range of slope between 0.97 and 1. These results indicate that the trained ANN model could accurately simulate the fluoride rejection as a function of permeate flux for the NF process dealing with fluoride removal.

4.3. Comparison of the ANN and NP-FT models

The experimental results predicted by both ANN and NP-FT models are compared in terms of coefficient of

determination (R^2). Table 4 shows the results obtained for the three membranes. According the results reported in Table 4 and the deviation of the predicted response values from the experimental data for both models illustrated in Fig. 10, both models show good and satisfactory R^2. However, the ANN model reveals a slight superiority over the NP-FT model. This slight prediction accuracy can be attributed to the general ability of ANNs to approximate the nonlinearity of the system [60,61]. In addition, ANNs have the advantage of flexibility and the ability to add new experimental data to build a more reliable ANN model [62], but, they have the disadvantage of providing little information about the membrane structures. In contrast the applied NP-FT model helps us to understand the transfer mechanism in the concentration polarization layer for the three membranes studied. In other words, both approaches are complementary to improve predictive modeling in the membrane system.

Table 4
ANN and NP-FT models comparison

Membrane	C_i (ppm)	R^2	
		ANN	NP-FT model
TR60	5	0.999	0.900
	10	0.999	0.900
	15	0.999	0.800
	20	0.999	0.880
NF270	5	0.819	0.700
	10	0.927	0.760
	15	0.884	0.750
	20	0.845	0.770
NF90	5	0.989	0.720
	10	0.999	0.700
	15	0.967	0.810
	20	0.999	0.818

The scatter plot of the predicted values of the NP-FT and ANN models vs. the actual values for the three tested membranes is presented in Fig. 10.

5. Conclusion

In this work, three NF membranes are studied on NaF-doped groundwater at different fluoride ion concentrations of which the experimental data are correlated and analyzed using two models (NP-FT and ANN).

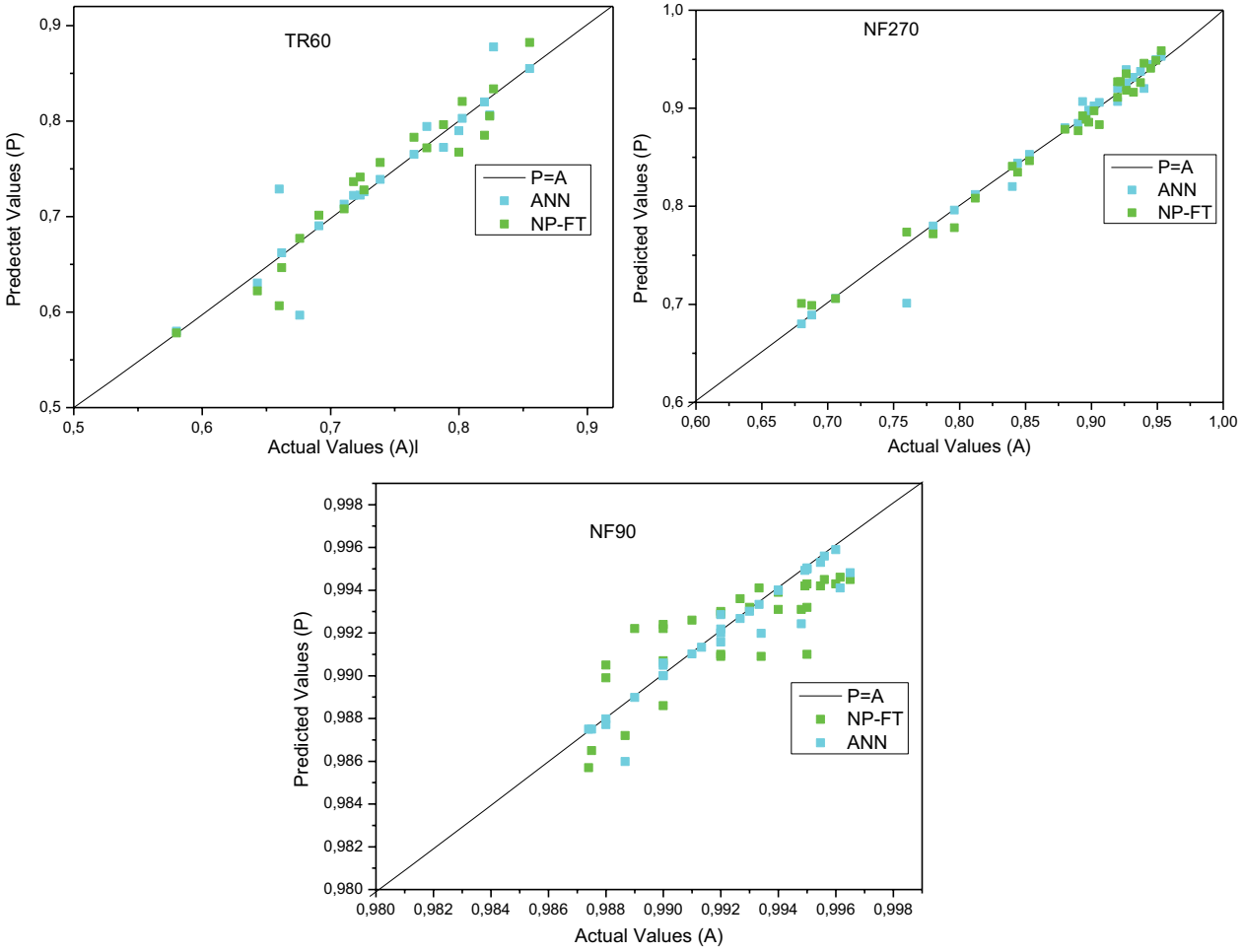

Fig. 10. Predicted values vs. actual values of ANN and NP-FT models for the three membranes.

According to the NP-FT model, the transfer mechanism of fluoride ions in NF membranes is studied and the obtained results show that σ are almost around (1–0.97–0.89) for the three membranes (NF90, NF270 and TR60) respectively. These values indicate that the transport is diffusive in NF90, while for TR60 and NF270 both mechanisms are present, but the predominance of diffusion is more pronounced for NF270 than for TR60. On the other hand, the thickness of the boundary layer formed by the gradient of fluoride ions is small and is about 10^{-5} m for NF270 and 10^{-6} m for TR60. In addition, the value obtained for the NF90 membrane is 10^{-14} m which, is very small, even non-existent. The greater the thickness of the boundary layer, the lower the permeability, and the permeability obtained follows the order below:

$$\text{TR60} > \text{NF270} > \text{NF90} \quad (15)$$

The ANN model shows a good agreement between the ANN prediction and the experimental data for all the studied membranes with a very low deviation. In terms of comparison between the two models used, the ANN model presents a superiority in the prediction of fluoride rejection, but this model gives no information neither on the mode of transfer, neither on the phenomena which intervenes in this transfer. On the opposite, the NP-FT model gives a good prediction, in addition to the determination of the phenomenological parameters to know (the coefficient of reflection σ, the permeability of the solute P_s, and the thickness of the boundary layer δ).

Symbols

P_i^*	—	Permeability of ion, m^2/s
P_s	—	Local solute permeability, m^2/s
C_f	—	Concentration in the membrane surface, mg/L
C_i	—	Concentration of ion, mg/L
C_p	—	Permeate concentration, mg/L
C_0	—	Feed concentration solution, mg/L
D_s	—	Effective diffusion coefficient of solute, m^2/s
F	—	Faraday constant, C/mol
J_s	—	Solute flux, $kg/m^3/m^2$ s
J_v	—	Volume flux, m^3/m^2 s
Q	—	Mass transfer coefficient in the boundary layer, m^3/m^2 s
R	—	Universal gas constant, J/K mol
R_{obs}	—	Observed solute retention, %
R_{real}	—	Real solute retention, %
T	—	Absolute temperature, K
x	—	Distance variable, m
Z_i	—	Ion valence number

Greek

σ	—	Reflection coefficient
δ	—	Thickness of the boundary layer, m
ψ	—	Electrostatic potential of the system, V
ξ	—	Error

References

[1] S. Ayoob, A.K. Gupta, V.T. Bhat, A conceptual overview on sustainable technologies for the defluoridation of drinking water, J. Crit. Rev. Env. Sci. Technol., 38 (2008) 401–470.

[2] M. Bodzeka, K. Konieczny, Fluorine in the water environment, Desal. Water Treat., 117 (2018) 118–141.

[3] M. Mohapatra, S. Anand, B.K. Mishra, D.E. Giles, P. Singh, Review of fluoride removal from drinking water, J. Environ. Manage., 91 (2009) 67–77.

[4] S. Selvakumar, K. Ramkumar, N. Chandrasekar, N.S. Magesh, S. Kaliraj, Groundwater quality and its suitability for drinking and irrigational use in the Southern Tiruchirappalli district, Tamil Nadu, India, J. Appl. Water Sci., 7 (2017) 411–420.

[5] S. Guiza, H. Hajji, M. Bagane, External mass transport process during the adsorption of fluoride from aqueous solution by activated clay, C.R. Chim., 22 (2019) 161–168.

[6] F. Wu, L. Feng, L. Zhang, Rejection prediction of isopropylantipyrine and antipyrine by nanofiltration membranes based on the Spiegler–Kedem–Katchalsky model, Desalination, 362 (2015) 11–17.

[7] A. Bhatnagar, E. Kumar, M. Sillanpää, Fluoride removal from water by adsorption – a review, J. Chem. Eng., 171 (2011) 811–840.

[8] H.N. Bhattacharya, S. Chakrabarti, Incidence of fluoride in the groundwater of Purulia District, West Bengal: a geoenvironmental appraisal, J. Curr. Sci., 101 (2011) 152–155.

[9] F.Z. Addar, S. El-Ghzizel, M. Tahaikt, M. Belfaquir, M. Taky, A. Elmidaoui, Fluoride removal by nanofiltration: experimentation, modelling and prediction based on the surface response method, Desal. Water Treat., 240 (2021) 75–88.

[10] M. Tahaikt, S. El-Ghzizel, N. Essafi, M. Hafsi, M. Taky, A. Elmidaoui, Technical-economic comparison of nanofiltration and reverse osmosis in the reduction of fluoride ions from groundwater: experimental, modeling and cost estimate, Desal. Water Treat., 216 (2021) 83–95.

[11] Y. Huang, X. Wang, Y. Xu, S. Feng, J.L.H. Wang, Amino-functionalized porous PDVB with high adsorption and regeneration performance for fluoride removal from water, Green Chem. Eng., (2020), doi: 10.1016/j.gce.2020.11.011 (in Press).

[12] S.V. Jadhav, K.V. Marathe, V.K. Rathod, A pilot scale concurrent removal of fluoride, arsenic, sulfate and nitrate by using nanofiltration: competing ion interaction and modelling approach, J. Water Process Eng., 13 (2016) 153–167.

[13] K. Wan, L. Huang, J. Yan, B. Ma, X. Huang, Z. Luo, H. Zhang, T. Xiao, Removal of fluoride from industrial wastewater by using different adsorbents: a review, Sci. Total Environ., 773 (2021) 145535, doi: 10.1016/j.scitotenv.2021.145535.

[14] X. Chen, C. Wan, R. Yu, L. Meng, D. Wang, W. Chen, T. Duan, L. Li, A novel carboxylated polyacrylonitrile nanofibrous membrane with high adsorption capacity for fluoride removal from water, J. Hazard. Mater., 411 (2021) 113–125.

[15] N. Drouiche, N. Ghaffour, S. Aoudj, M. Hecini, T. Ouslimane, Fluoride removal from photovoltaic wastewater by aluminium electrocoagulation and characteristics of products, J. Chem. Eng. Trans., 17 (2009) 1651–1656.

[16] N. Boudjema, N. Abdi, H. Grib, N. Drouiche, H. Lounici, N. Mameri, Simultaneous removal of natural organic matter and turbidity from Oued El Harrach River by electrocoagulation using an experimental design approach, Desal. Water Treat., 57 (2015) 14386–14395.

[17] S. Chakrabortty, M. Roy, P. Pal., Removal of fluoride from contaminated groundwater by cross flow nanofiltration: transport modeling and economic evaluation, Desalination, 313 (2013) 115–124.

[18] M. Tahaikt, F. Elazhar, I. Mohamed, H. Zeggar, M. Taky, A. Elmidaoui, Comparison of the performance of three nanofiltration membranes for the reduction of fluoride ions: application of the Spiegler–Kedem and steric hindrance pore models, Desal. Water Treat., 240 (2021) 14–23.

[19] M. Tahaikt, A. Ait Haddou, R. El Habbani, Z. Amor, F. Elhannouni, M. Taky, M. Kharif, A. Boughriba, M. Hafsi,

A. Elmidaoui, Comparison of the performances of three commercial membranes in fluoride removal by nanofiltration. Continuous operations, Desalination, 225 (2008) 209–219.
[20] J. Shen, A.I. Schafer, Factors affecting fluoride and natural organic matter (NOM) removal from natural waters in Tanzania by nanofiltration/reverse osmosis, Sci. Total Environ., 527–528 (2015) 520–529.
[21] A. Fatehizadeh, M.M. Amin, M. Sillanpää, N. Hatami, E. Taheri, N. Baghaei, S. Mahajan, Modeling of fluoride rejection from aqueous solution by nanofiltration process: single and binary solution, Desal. Water Treat., 193 (2020) 224–234.
[22] M. Pontié, H. Buisson, C.K. Diawara, H. Essis-Tome, Studies of halide ions mass transfer in nanofiltration – application to selective defluorination of brackish drinking water, Desalination, 157 (2003) 127–134.
[23] A.B. Nasr, C. Charcosset, R.B. Amar, K. Walha, Defluoridation of water by nanofiltration, J. Fluorine Chem., 150 (2013) 92–97.
[24] A. Mnif, M. Ben Sik Ali, B. Hamrouni, Effect of some physical and chemical parameters on fluoride removal by nanofiltration, Ionics, 16 (2010) 245–253.
[25] H. Al-Zoubi, N. Hilal, N.A. Darwish, A.W. Mohammad, Rejection and modelling of sulphate and potassium salts by nanofiltration membranes: neural network and Spiegler–Kedem model, Desalination, 206 (2007) 42–60.
[26] L.B. Chaudhari, Z.V.P. Murthy, Separation of Cd and Ni from multicomponent aqueous solutions by nanofiltration and characterization of membrane using IT model, J. Hazard. Mater., 180 (2010) 309–315.
[27] H. Kelewou, A. Lhassani, M. Merzouki, P. Drogui, B. Sellamuthu, Salts retention by nanofiltration membranes: physicochemical and hydrodynamic approaches and modeling, Desalination, 277 (2011) 106–112.
[28] M. Jarzyńska, M. Pietruszka, The application of the Kedem–Katchalsky equations to membrane transport of ethyl alcohol and glucose, Desalination, 280 (2011) 14–19.
[29] D. Meng, B. Zheng, G. Lin, M.L. Sushko, Numerical solution of 3D Poisson–Nernst–Planck equations coupled with classical density functional theory for modeling ion and electron transport in a confined environment, Commun. Comput. Phys., 16 (2014) 1298–1322.
[30] T. Chaabane, S. Taha, M.T. Ahmed, R. Maachi, G. Dorange, Coupled model of film theory and the Nernst–Planck equation in nanofiltration, Desalination, 206 (2007) 424–432.
[31] X. Hua, H. Zhao, R. Yang, W. Zhang, W. Zhao, Coupled model of extended Nernst–Planck equation and film theory in nanofiltration for xylo-oligosaccharide syrup, J. Food Eng., 100 (2010) 302–309.
[32] J. Fang, B. Deng, Rejection and modeling of arsenate by nanofiltration: contributions of convection, diffusion and electromigration to arsenic transport, J. Membr. Sci., 453 (2014) 42–51.
[33] M. Hamachi, M. Cabassud, A. Davin, M.M. Peuchot, Dynamic modelling of crossflow microfiltration of bentonite suspension using recurrent neural networks, Chem. Eng. Process., 38 (1999) 203–210.
[34] W.R. Bowen, M.G. Jones, H.N. Yousef, Dynamic ultrafiltration of proteins — a neural network approach, J. Membr. Sci., 146 (1998) 225–235.
[35] W. Richard Bowen, M.G. Jones, H.N.S. Yousef, Prediction of the rate of crossflow membrane ultrafiltration of colloids: a neural network approach, Chem. Eng. Sci., 53 (1998) 3793–3802.
[36] N. Delgrange, C. Cabassud, M. Cabassud, L. Durand-Bourlie, J.M. Lainé, Modelling of ultrafiltration fouling by neural network, Desalination, 118 (1998) 213–227.
[37] N. Delgrange, C. Cabassud, M. Cabassud, L. Durand-Bourlie, J.M. Lainé, Neural network for prediction of ultrafiltration transmembane pressure — application to drinking water, J. Membr. Sci., 150 (1998) 111–123.
[38] C. Teodosiu, O. Pastravanu, M. Macoceanu, Neural network model for ultrafiltration and backwashing, J. Water Res., 34 (2000) 4371–4380.
[39] W.R. Bowen, M.G. Jones, J.S. Welfoo, H.N.S. Yousef, Predicting salt rejections at nanofiltration membranes using artificial neural networks, Desalination, 129 (2000) 147–162.
[40] Guidelines for Drinking-Water Quality: Fourth Edition Incorporating the First Addendum, World Health Organization, Geneva, 2017. Licence: CC BY-NC-SA 3.0IGO; Available at: https://creativecommons.org/licenses/by-nc-sa/3.0/igo.
[41] Moroccan Official Bulletin, Joint Orders No. 1275-01, 1276-01 and 1277-01 of 17th October 2002 Defining the Quality Norms of Surface Waters, Waters Destined for Irrigation and of Surface Waters Used for the Production of Drinking Water Respectively, Official Bulletin of the Kingdom of Morocco, Moroccan Official Bulletin: Rabat, Morocco, 2002, pp. 1518–1525.
[42] M.A. Menkouchi Sahli, S. Annouarb, M. Tahaikt, M. Mountadar, A. Soufiane, A. Elmidaoui, Fluoride removal for underground brackish water by adsorption on the natural chitosan and by electrodialysis, Desalination, 212 (2007) 37–45.
[43] M. Pontie, H. Dach, A. Lhassani, C.K. Diawara, Water defluoridation using nanofiltration vs. reverse osmosis: the first world unit, Thiadiaye (Senegal), Desal. Water Treat., 51 (2013) 164–168.
[44] J. Guo, H. Bao, Y. Zhang, X. Shen, J.-K. Kim, J. Ma, L. Shao, Unravelling intercalation-regulated nanoconfinement for durably ultrafast sieving graphene oxide membranes, J. Membr. Sci., 619 (2021) 118791, doi: 10.1016/j.memsci.2020.118791.
[45] K. Boussu, Y. Zhang, J. Cocquyt, P. Van der Meeren, A. Volodin, C. Van Haesendonck, J.A. Martens, B. Van der Bruggen, Characterization of polymeric nanofiltration membranes for systematic evaluation of membrane performance, J. Membr. Sci., 278 (2006) 418–427.
[46] H. Moayedi, B. Aghel, B. Vaferi, L.K. Foong, D.T. Bui, The feasibility of Levenberg–Marquardt algorithm combined with imperialist competitive computational method predicting drag reduction in crude oil pipelines, J. Pet. Sci. Eng., 185 (2020) 106634, doi: 10.1016/j.petrol.2019.106634.
[47] S.A. Taqvi, L.D. Tufa, H. Zabiri, A.S. Maulud, F. Uddin, Fault detection in distillation column using NARX neural network, Neural Comput. Appl., 32 (2020) 3503–3519.
[48] L. Dresner, Some remarks on the integration of the extended Nernst–Planck equations in the hyperfiltration of multicomponent solutions, Desalination, 10 (1972) 27–46.
[49] L. Song, M. Elimelech, Theory of concentration polarization in cross-flow filtration, J. Chem. Soc., Faraday Trans., 19 (1995) 3389–3398.
[50] J.M. Pope, S. Yao, A.G. Fane, Quantitative measurements of the concentration polarization layer thickness in membrane filtration of oil-water emulsions using NMR micro-imaging, J. Membr. Sci., 118 (1996) 247–257.
[51] R. Bian, K. Yamamoto, Y. Watanabe, The effect of shear rate on controlling the concentration polarization and membrane fouling, Desalination, 131 (2000) 225–236.
[52] S. Lee, Y. Shim, S. Kim, J. Sohn, S.K. Yim, J. Cho, Determination of mass transport characteristics for natural organic mater in ultrafiltration and nanofiltration membranes, Water Sci. Technol. Water Supply, 2 (2002) 151–160.
[53] l. Nghiem, A. Schäfer, M. Elimelich, Removal of natural hormones by nanofiltration membranes: measurement, modelling, and mechanisms, J. Environ. Sci. Technol., 38 (2004) 1888–1896.
[54] J. Mallevialle, P.E. Odendaal, M.R. Wiesner, Water Treatment Membrane Processes, McGraw Hill, New York, 1996.
[55] B. Sarkar, A. Sengupta, S. De, S. DasGupta, Prediction of permeate flux during electric field enhanced cross-flow ultrafiltration—a neural network approach, Sep. Purif. Technol., 65 (2009) 260–268.
[56] L. Zhao, W. Xia, H. Zhao, J. Zhao, Study and modeling of the separation characteristics of a novel alkali-stable NF membrane, Desal. Water Treat., 20 (2010) 253–263.
[57] M. Khayet, C. Cojocaru, M. Essalhi, Artificial neural network modeling and response surface methodology of desalination by reverse osmosis, J. Membr. Sci., 368 (2011) 202–214.

[58] N.B. Shaik, S.R. Pedapati, S.A.A. Taqvi, A.R. Othman, F.A.A. Dzubir, A feed-forward back propagation neural network approach to predict the life condition of crude oil pipeline, Processes, 8 (2020) 661, doi: 10.3390/pr8060661.
[59] L. Xu, X. Gao, Z. Li, C. Gao, Removal of fluoride by nature diatomite from high-fluorine water: an appropriate pretreatment for nanofiltration process, Desalination, 369 (2015) 97–104.
[60] P. Singh, S.S. Shera, J. Banik, R.M. Banik, Optimization of cultural conditions using response surface methodology versus artificial neural network and modeling of L-glutaminase production by *Bacillus cereus* MTCC 1305, J. Bioresour. Technol., 137 (2013) 261–269.
[61] K.M. Desai, S.A. Survase, P.S. Saudagar, S.S. Lele, R.S. Singhal, Comparison of artificial neural network (ANN) and response surface methodology (RSM) in fermentation media optimization: case study of fermentative production of scleroglucan, J. Biochem. Eng., 41 (2008) 266–273.
[62] F. Geyikci, E. Kılıc, S. Coruh, S. Elevli, Modelling of lead adsorption from industrial sludge leachate on red mud by using RSM and ANN, J. Chem. Eng., 183 (2012) 53–59.